Int J Mech Mater Des
DOI 10.1007/s10999-007-9041-3

Modeling the brittle–ductile transition in ferritic steels: dislocation simulations

S. J. Noronha · N. M. Ghoniem

Received: 24 May 2007 / Accepted: 19 July 2007

Abstract We present a model for the brittle–ductile transition in ferritic steels based on two dimensional discrete dislocation simulations of crack-tip plasticity. The sum of elastic fields of the crack and the emitted dislocations defines an elasto–plastic crack field. Effects of crack-tip blunting of the macrocrack are included in the simulations. The plastic zone characteristics are found to be in agreement with continuum models, with the added advantage that the hardening behavior comes out naturally in our model. The present model is composed of a macrocrack with microcracks ahead of it in its crack-plane. These microcracks represent potential fracture sites at internal inhomogeneities, such as brittle precipitates. Dislocations that are emitted from the crack-tip account for plasticity. When the tensile stress along the crack plane attains a critical value σ_F over a distance fracture is assumed to take place. The brittle–ductile transition curve is obtained by determining the fracture toughness at various temperatures. Factors that contribute to the sharp upturn in fracture toughness with increasing temperature are found to be: the increase in dislocations mobility, and the decrease in tensile stress ahead of the macrocrack tip due to increase in blunting, and the slight increase in fracture stress of microcracks due to increase in plasticity at the microcrack. The model not only predicts the sharp increase in fracture toughness near the brittle–ductile transition temperature but also predicts the limiting temperature above which valid fracture toughness values cannot be estimated; which should correspond to the ductile regime. The obtained results are in reasonable agreement when compared with the existing experimental data.

Keywords Fracture · Brittle–ductile transition · Ferritic steels · Dislocation simulation

S. J. Noronha (✉) · N. M. Ghoniem
Department of Mechanical and Aerospace Engineering, University of California, Los Angeles, CA 90095-1597, USA
e-mail: silvester.noronha@areva.com

Present Address:
S. J. Noronha
NSSS Mechanical Engineering Department, AREVA NP Inc, 3315 Old Forest Road, Lynchburg, VA 24506, USA

1 Introduction

Brittle–ductile transition in ferritic steels undoubtedly has significant economical and technological importance as a result of the widespread applications of these steels in nuclear pressure vessels, power plants, hydrogen tanks, etc. Since the introduction of crack-tip plasticity models for Brittle–Ductile Transition (BDT) (Rice and Thomson 1974), interest in the study of the phenomenon continued in the literature (Rice 1992; Hirsch et al. 1989; Hirsch and Roberts 1991, 1997). Rice and Thomson (1974) were the first

to analyze the problem; by equating the competing forces acting on a dislocation near the crack-tip, and derived a relation for the intrinsic brittleness or ductility of a material based the dislocation core width and other material parameters. Rice (1992) further refined these conditions by obtaining the critical loadings for dislocation emission and cleavage. He equated the crack-tip driving forces on distributed shear dislocation cores and cleavage opening, respectively, to the local resistance of dislocation propagation and cleavage along the slip/crack plane. The process (either emission or further opening), which has equal driving force and resistance at the lowest applied load, determines the failure mode. Failure is thus controlled by two material parameters, the surface energy (γ) and the unstable stacking fault energy (γ_{us}) (Rice 1992). With increasing computational power, numerical models have been introduced at the discrete dislocation dynamics and molecular dynamics levels. Notable among the dislocation dynamics based efforts is the model introduced by Hirsch and Roberts (Hirsch et al. 1989; Hirsch and Roberts 1997) to study the effect of dislocation mobility and dislocation source configurations on the BDT of Si.

Despite these advances in understanding the BDT of simple single crystalline materials, the prediction of BDT of practical materials like steels still relies heavily on empirical and continuum methods that embody constitutive laws. It is well accepted now that the fracture of ferritic steels at low temperatures range where it propagates by cleavage, originate in microcracks (mostly in precipitates) ahead of a dominant macrocrack. The dominant macrocrack may be intentionally introduced by pre-cracking a test specimen or may exist as a surface crack in practical structures. The high value of the fracture toughness in ferritic steels (>30 MPa$\sqrt{\text{m}}$ in the cleavage regime; compared to 1 MPa$\sqrt{\text{m}}$ calculated from surface energy considerations alone) is attributed to the observation that cleavage is initiated from microcracks ahead of the macrocrack (Orowan 1945). Experiments have showed that these microcracks mostly originate in precipitates (McMahon and Cohen 1965; Bowen et al. 1987), and the propagation of these microcracks is the *controlling step* in the fracture of ferritic steels (McMahon and Cohen 1965; Ritchie et al. 1973; Curry and Knott 1979). Thus, cleavage fracture in steels can be considered as a two step fracture process: (1) the generation of microcracks as a result of stress concentrations at the non-deformable particles generated by local plastic flow in the matrix, (2) the propagation of these microcracks in the matrix. Based on numerous experimental evidences (e.g. McMahon and Cohen 1965; Ritchie et al. 1973; Curry and Knott 1979), it is now widely accepted that the *critical step* in such two-step fracture process is the second step or the propagation of microcracks. For this reason, in this paper we model and simulate the condition for propagation of microcracks. The dislocation simulation method has recently been used to model the initiation of cleavage of ferritic steels at low temperature (Roberts et al. 2002). A finite slit crack, loaded under triaxial stress, is used to study the cleavage initiated by brittle precipitates. The model predicts the near constancy of the microscopic cleavage fracture stress (σ_F) with temperature observed in many experiments and has showed reasonable quantitative agreement with experiments (Bowen et al. 1987).

Ritchie, Knott and Rice (RKR) (Ritchie et al. 1973) used solutions based on Hutchinson, Rice and Rosengren (HRR) (Hutchinson 1968; Rice and Rosengren 1968) and Finite Element Analysis (FEA) to simulate the plastic zone. In these simulations, a critical tensile stress achieved over a characteristic *distance* ahead of the crack is used as an appropriate failure criterion. This *distance* is essentially a fitting parameter and RKR (Ritchie et al. 1973) used a value equal to twice the average grain diameter. The model successfully predicts the lower-shelf fracture toughness, but fails to predict the sharp increase with temperature near the transition temperature. Statistical models have also been introduced to predict the brittle–ductile transition in steels (e.g. Curry and Knott 1979; Beremin 1983; Wallin et al. 1984) where the statistical aspect of cleavage fracture in practical steel was recognized. In these models, FEA solutions of crack-tip plasticity were used to obtain the stress fields ahead of the crack. In the Beremin model (Beremin 1983), the maximum principal stress is calculated for each volume element in the plastic zone and a probability of failure is assigned. The total probability of failure is then obtained by summing over the entire plastic zone. Wallin et al. (Wallin et al. 1984), extended the model to the transition region by using and empirical relation for the

variation of the *effective surface energy* ($\gamma_s + \gamma_p$) with temperature, where γ_s is the true surface energy and γ_p the plastic work done during propagation. This eventually led to the Master Curve (MC) hypothesis, which states that the brittle–ductile transition of all ferritic steels follows a universal curve (Wallin et al. 1984; Wallin 1993). Even though the MC is used to check the reliability of structures under irradiation (ASTM Standard Test Method 2002), a clear understanding of the physical basis of this methodology is still lacking (Natishan and Kirk 2000). Odette and He (2000) explained the master curve using a microscopic fracture stress (σ_F) that remains constant at low temperatures and increase at higher temperatures. Some experimental findings (Bowen et al. 1987; Ortner and Hippsley 1996) indicate that the fracture stress is not sensitive to temperature, and more careful experiments and simulations may be required to determine the temperature dependence of σ_F. Here we find a slight increase in σ_F with temperature, but quite different from what is assumed by Odette et al. (Odette and He 2000).

As mentioned earlier, discrete dislocation simulations of crack-tips were successful in predicting the brittle–ductile transition (BDT) of simple single crystalline materials (e.g. Hirsch et al. 1989; Hirsch and Roberts 1991). The advantage of this approach over continuum methods is that fundamental material behavior, such as change in dislocation velocity and the mutual interactions of dislocations can be treated dynamically. By these simulations, it has been found that the dislocation mobility plays a significant role in determining the transition temperature (Hirsch et al. 1989; Hirsch and Roberts 1991). However, the variation of dislocation mobility alone cannot explain the BDT behavior in multiphase materials. An earlier attempt to model the BDT of complex materials like steels (Hirsch and Roberts 1997) predicted the lower shelf fracture toughness substantiating the Orowan's postulate (Orowan 1945) on high fracture toughness measured at low temperature. However, the model failed to predict the sharp increase of fracture toughness around the transition temperature region. Recently we introduced a model including the effects of macrocrack-tip blunting and a preliminary analysis was reported in (Noronha et al. 2006).

Here, we present a discrete dislocation simulation, where the following features are introduced: (a) the plasticity at the microcrack tip, (b) macrocrack-tip blunting; the distance of the critical microcrack from the notional crack-tip is related to the radius of curvature of the blunted macrocrack tip. In the following section, we outline the detailed procedure of the methodology used in the present simulation. Then in Sect. 3, we present a detailed analysis of the simulated crack-tip plastic zone. In Sect. 4, we discuss the results and analysis of fracture toughness calculations. We further compare our predictions with experimental results reported in the literature. Finally, we summarize the results and discuss implications of our model.

2 Model and method of calculation

2.1 Overview

From the results of numerous experiments conducted on the fracture of steels it is now established that: (a) the measured microscopic fracture stress (at microcracks) is found to be substantially higher than that of the pure Griffith value for pure iron (Bowen et al. 1987; Ortner and Hippsley 1996); (b) several cracked brittle particles are found to be present in broken samples (Bowen et al. 1987; Ortner and Hippsley 1996; Bowen and Knott (1986); consequently it is concluded that the critical step in the fracture processes is the spread of cleavage from one of the cracked particles; (c) pre-cracks (macrocracks) blunt substantially before the fracture of the specimen occurs at the transition region. However, examination of the fracture surface reveals that cracks propagate predominantly by cleavage (Veistinen and Lindroos 1984; Bowen et al. 1986), (d) Stress fields obtained by finite element analysis of blunted crack on elastic-plastic material shows that the tensile stress ahead of the crack on the crack plane has a maxima at some distance ahead of the crack-tip (McMeeking 1977). Based on these observations, the present model has the following features:

(1) At the microcrack, the emission of dislocations and subsequent shielding of the microcrack-tip (a detailed study of this and the observed constancy for microscopic fracture stress is reported in an earlier study (Roberts et al. 2002).
(2) A microcrack in the field of macrocrack; the failure criterion is the cleavage crack propagation from the microcrack.

(3) Blunting of the macrocrack resulting from dislocation emission; we therefore use the elastic crack-tip stress field for blunted cracks.
(4) The position of the microcrack is assumed to be ahead of the crack at a constant distance with respect to the blunted macrocrack tip.

As shown schematically in Fig. 1, the macrocrack is assumed to be semi-infinite, with dislocation sources close to the crack-tip. Dislocations are emitted simultaneously along two slip planes, symmetrically oriented to the crack plane and inclined at an angle, α to the crack plane. As the load is increased, dislocations are emitted and the crack-tip gets blunted, which is schematically illustrated in Fig. 1b. As blunting increases:

(a) The crack tip fields are modified to be that of a blunted crack (Creager and Paris 1967).
(b) The source position (x_0) with respect to the centre of curvature of the blunted crack along the slip plane is selected to be equal to the crack-tip radius, i.e. $x_0 = \rho + 4b$ when $\rho > 4b$, where b is the magnitude of Burgers vector (initial x_0 is chosen to be $4b$ following an earlier study) (Roberts et al. 2002). The radius of the blunted crack, ρ, is taken to be equal to N b sinα, where N is the number of dislocations and α is the slip plane angle.
(c) The notional crack-tip from which the image stresses of dislocations are calculated is always located at the center of curvature of the blunted crack.

The plastic zone developed by the arrays of emitted dislocations from the macrocrack modifies the field ahead of it to that of an elastic–plastic material with hardening. During loading, dislocations are emitted from source positions when the resolved shear stress reaches a value τ_y, where τ_y is the *mean friction stress* experienced by dislocations and may be due to the effect of all types of obstacles in dislocation motion including impurities, precipitates, grain boundaries, etc, in addition to the lattice friction. The resolved shear stress (τ_i) is obtained using expressions based on derivations for finite crack (Wang and Lee 1990), and semi-infinite crack (Lakshmanan and Li 1988) for respective cases. An emitted dislocation (i) moves on the respective slip with a velocity:

$$v_i = \left(\frac{\tau_i - \tau_y}{\tau_i}\right)\left(\frac{\tau_i}{\tau_0}\right)^m v_0 \qquad (1)$$

when $|\tau_i| > \tau_y$, and $v_i = 0$ when $|\tau_i| < \tau_y$, with

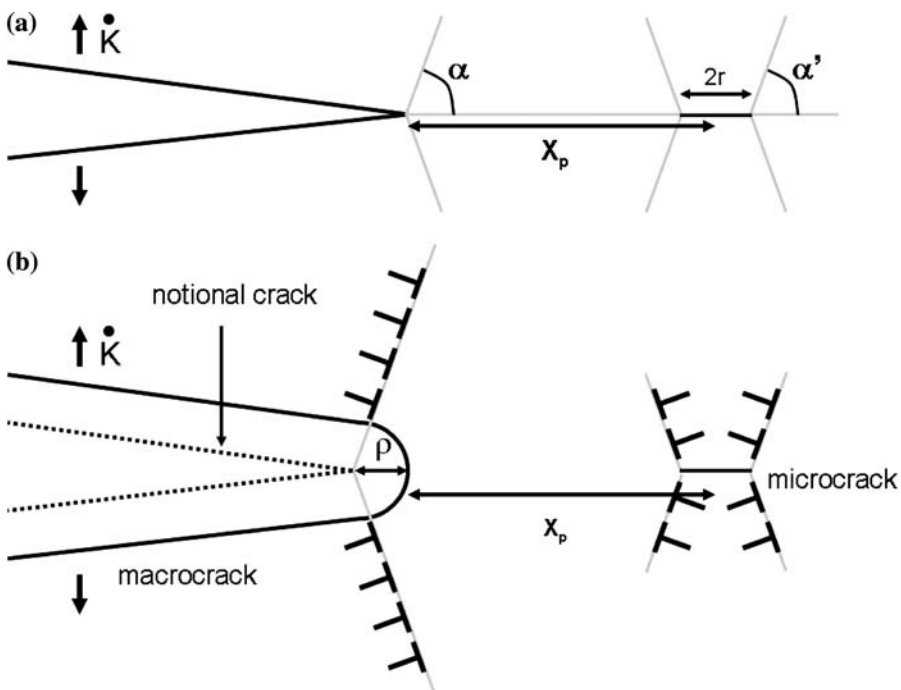

Fig. 1 (**a**) The geometry of the crack and slip planes used in the macrocrack–microcrack simulation model. The slip planes angles are oriented at α and α' to the crack planes of macrocrack and microcrack respectively, $2r$ is the microcrack size and X_P, the distance of the microcrack from macrocrack tip. K is the applied load at the macrocrack. (**b**) Schematic illustration of crack-tip blunting. ρ is the radius of the blunted crack-tip, The distance of the microcrack from center of curvature of the blunted crack increases from X_p to $X_p + \rho$

$m = 2.67$ and $v_0 = 4.545 \times 10^{-10}$ ms^{-1} and $\tau_0 = 1$ MPa estimated based on dislocation velocity measurements (Saka et al. 1973). Since the dislocations move only when $|\tau_i| > \tau_y$ they are in their equilibrium positions at any given time. We used a constant value of v_0 for all temperatures so that equilibrium configuration could be reached faster at low temperatures. Since we seek the equilibrium distribution of dislocations at each case, the temperature and strain rate dependence of measured fracture toughness (K_F), plastic zone size (d_F), crack-tip opening displacement, etc. are determined only by the temperature and strain-rate dependence of the *mean friction stress* (τ_y). In turn, τ_y is chosen to be equal to shear yield stress $\sigma_y/2$ assuming the material to follow the Tresca yield criterion. The σ_y is the measured uniaxial yield stress at a given temperature. Alternatively, we can use other relations to relate uniaxial yield stress to shear yield stress (Stoller and Zinkle 2000). However, they differ only in a numerical constant and hence the results should hold for any relation used. The temperature-yield stress relation used throughout this paper is obtained from the Zerilli-Armstrong equations for BCC Fe (Zerilli and Armstrong 1986), the calculated yield stress or flow stress dependence is shown in Fig. 2. Thus, the temperature dependence of fracture toughness is obtained by inputting the corresponding mean friction stress value for each temperature. For our simulations, the yield stress (σ_y) varies from 1200 to 200 MPa, corresponding to temperatures ranging from 30 to 400 K. The load is incremented at a rate dK/dt (= 0.01 MPa$\sqrt{\text{m}}$ s^{-1}); a variable time step is used to assume that dislocations move as an array, and numerical instabilities are avoided. Also once the dislocations are moved far away from the crack-tip we use "bundling of dislocations" (Roberts 1996) to speed up the computation.

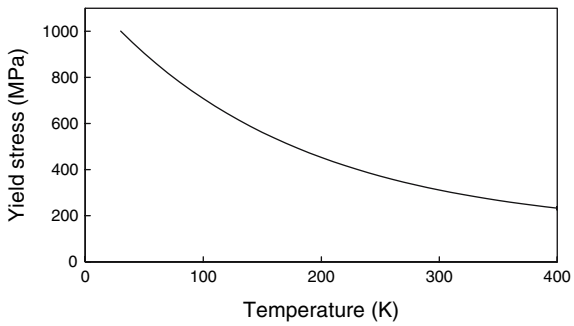

Fig. 2 The flow stress as a function of temperature for BCC iron calculated from Zerelli-Armstrong (1986)

Our simulations are preformed in two stages: the microcrack is first loaded to failure and the microscopic fracture stress (σ_F) is estimated. The obtained microscopic fracture stress (σ_F) values are then used as the fracture criterion in the macrocrack simulation.

2.2 Microcrack simulation: calculation of microscopic fracture stress (σ_F)

A finite through thickness crack with dislocation sources located on four slip planes oriented at angles symmetric to crack planes at both crack-tips is used. The configuration is shown on the right hand side of Fig. 1. The criterion for dislocation emission is that the total shear stress acting on a dislocation at the source position, including the crack tip field stress, the direct stress and image stress due to dislocations. The crack-tip stress field derived for mode-I slit crack in (Wang and Lee 1990) consists of the K-field from the loaded finite crack and the far field applied stress. But, here we consider the microcrack situated in the plastic-zone ahead of a loaded semi-infinite maro-crack. In this case in plain strain the "applied" stress field acting on the microcrack is triaxial. As a first approximation we describe the stress state in the plastic zone under plane strain conditions, ahead of the marcocrack-tip as a superposition of hydrostatic tensile stress and a shear stress ($\sigma_y/2$) at 45° to the x–y axes. The shear stress is equivalent to a tensile stress of ($\sigma_y/2$) normal to the crack plane (y-axis), and a compressive stress ($-\sigma_y/2$) in the crack plane normal to the crack front (x-axis). Since the components of stress field parallel to the plane of the microcrack do not affect the strength of the K-field, the total strength generating the K-field can be represented as a tensile stress ($\sigma^a = \sigma_h + \sigma_y/2$) along the y-axis normal to the plane of the microcrack. On the other hand, the non-K filed stress which causes slip directly is the shear stress $\sigma_y/2$ at 45° to the x, y axis, which is equivalent to a uniaxial yield stress σ_y along the y-axis. This mimic the triaxial stress field at the microcrack embedded in the plastic zone of a macrocrack. In the expressions for the stress fields given in (Wang and Lee 1990) we replaced the tensile component of far field stress (σ^a) with the uniaxial

yield stress (σ_y) for instances when $\sigma^a > \sigma_y$ (that is when the material is yielded). Thus the simulations with $\sigma^a > \sigma_y$ represent the development of plasticity around the microcrack in the plastic zone of the semi-infinite macrocrack.

On loading, edge dislocations are emitted when the resolved shear stress at the source positions exceed τ_y. The emitted dislocations move with the velocity law described in equation (1); once moved to their equilibrium positions the amount of shielding (k_d) from these dislocations at the crack-tip are calculated using expressions derived in (Wang and Lee 1990). The emitted dislocations shield the crack tip from external loading, thereby enhancing the stress needed for the crack to propagate. The microcrack propagates when the crack-tip stress intensity (k) exceeds a pre-assigned critical value, $k = k_a – k_d = K_{Ic}$, where k_a is the "applied" stress intensity factor and k_d is the stress intensity factor due to all the dislocations at the microcrack tip. Here the value of K_{Ic} is chosen to be that for cleavage of pure iron which is found to be 1 MPam$^{1/2}$. The applied load ($\sigma_A = k_a/\sqrt{\pi r}$, r is the half-width of microcrack) at fracture is the microscopic fracture stress (σ_F).

2.3 Macrocrack simulation: calculation of fracture toughness (K_F)

A schematic illustration of the macrocrack simulation is shown on the left hand side of Fig. 1. A semi-infinite crack, with dislocation sources at x_0 (x_0 is chosen as described in Sect. 2.1) is loaded. Dislocations are emitted simultaneously along the two slip planes, symmetrically oriented to the crack plane. The slip plane angle fore detailed simulations are chosen to be 70.5°; the direction of maximum shear stress of the elastic crack-tip field. As we demonstrate in the next section, the slip plane angle 70.5° matches best with continuum estimates. During the simulation, the applied stress intensity is increased in small increments and the equilibrium positions of dislocations are determined. As the load is increased, more and more dislocations are emitted and the macrocrack gets blunted. At each time step, the stress ahead of the macrocrack at distance X_p (the microcracks are assumed to be at this position) along the crack plane is calculated using the expressions derived in (Lakshmanan and Li 1988). Fracture is assumed to occur when the tensile stress (σ^p_{yy}) at distance X_p (at the particle) reaches σ_F. The applied load at the macrocrack, when the fracture criterion is satisfied is the stress intensity at fracture (K_F) or fracture toughness. The calculation is repeated for yield stresses ranging from 300 to 1200 MPa corresponding to temperatures from 350 to 25 K. Throughout the simulation, a microcrack of size 2.5 μm is used; this value is chosen as a typical maximum value in the range of sizes of microcracks found in experiments (Roberts et al. 2002). The detailed simulations reported here are obtained using X_p = 10 μm. These values of microcrack size and its distance from the crack were chosen as typical values of largest microcrack size and smallest grain size in this type of steels. It should be noted these typical (mean) values are strictly valid only if the sampling space is large enough or the microstructure is homogenous. However, the sampling may not be large enough and may be the reason for commonly observed scatter in the measurement of fracture toughness. However, it should be noted that if we average a sufficient number of values, the functional form of the variation of fracture toughness with temperature will follow the mean curve corresponding to the one we estimate here.

3 Results and discussion

3.1 Analysis of crack-tip plastic zones

Figure 2 shows the dependence of the yield stress on temperature obtained from Zerilli-Armstrong model using parameters for BCC Fe (Zerilli and Armstrong 1986). This temperature dependence data was used for all the simulations presented in this paper unless mentioned otherwise. The flow stress is calculated using $\sigma = c_1 \exp(-c_3 T + c_4 T \ln \dot{\varepsilon}) + c_5 \varepsilon^n$ where, c_1 = 1033 MPa, c_3 = 0.00698 (K^{-1}), c_4 = 0.000415 (K^{-1}), $\dot{\varepsilon}$ = 407 c_5 = 2.66 MPa, ε = 0.01, n = 0.289. Figures 3a and b show the normalized tensile stress field ahead of the crack, along the crack-plane as a function of the normalized distance from the crack-tip. The curves represent the stress field for an applied K = 20 MPa$\sqrt{\text{m}}$. It should be noted that the stress fields beyond a normalized distance of 0.1–1.0 from the tip asymptotes to the elastic field and decay as $X^{-1/2}$. The distance at which the elastic behavior is resumed marks the end of projection of plastic zone

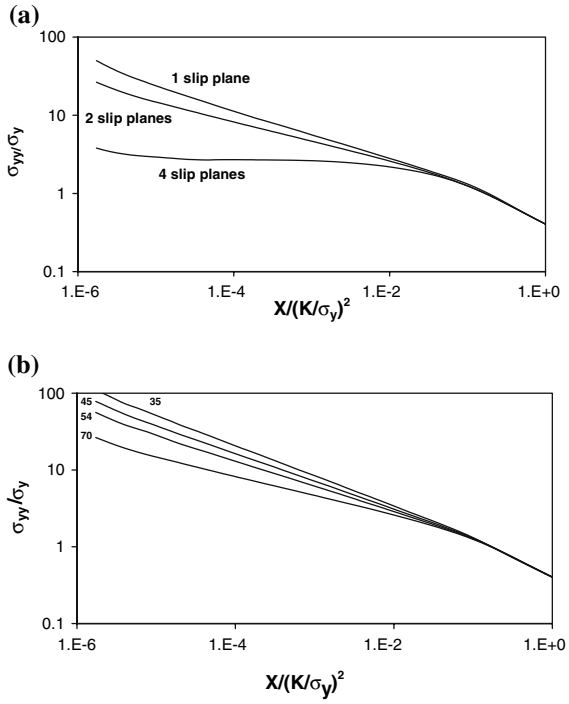

Fig. 3 (**a**) The normalized tensile stress ahead of the crack-tip as a function of normalized distance from the crack-tip for different number of slip planes. (**b**) The normalized tensile stress ahead of the crack-tip as a function of normalized distance from the crack-tip for four different slip planes angles; the numbers represent the angles used. For each case two symmetric slip planes are used

size on the crack plane. Figure 3a shows the stress field calculated for three different slip plane configurations: (a) for a single slip plane case, one slip intersecting the crack tip and oriented at an angle 70° to the crack plane; (b) for two slip planes, the slip planes are symmetric to the crack plane (as shown schematically in Fig. 1); (c) configuration for 4 slip planes case, the slip planes are symmetric to the crack plane and are oriented at $\alpha = \pm 110°, \pm 70.5°$. Assuming that these curves have power-law dependence on the distance from the crack tip (r^{-N}), we fit these points with a power-law and the exponents are found to be $N = 0.32$ and 0.25, respectively, for the single and double slip plane cases. For the 4 slip plane case, there is hardly any region of power-law dependence; the decay of stress field is rather nearly flat. The HRR (Hutchinson 1968; Rice and Rosengren 1968) field is characterized using, $\sigma_{\mathrm{HRR}} \sim \mathrm{X}^{-\mathrm{n}/(\mathrm{n}+1)}$, where n is the hardening exponent of the material. Therefore, the exponents of the stress field variation in our model is related to the hardening exponent as n/n + 1 = N. Thus, the hardening exponent in the case of single slip plane is 0.5, and that of two slip plane case is 0.33. The value of two slip plane (0.33) is closer to the value obtained experimentally for strain hardening exponent for this type of steel. Thus the agreement with continuum models has substantially improved compared to previous estimations from an asymmetric single slip plane cases (e.g. Hirsch and Roberts 1997). In Fig. 3b, the effect of slip plane angle is shown. The hardening exponents for three crystallographically relevant (for BCC Fe) angles along with the maximum shear stress direction (70.5°) are shown. The exponents of power law variation of stress field along the crack-plane for slip plane angles, 35, 45, 54 and 70.5° are, 0.396, 0.365, 0.335 and 0.252 respectively, and the corresponding hardening exponents are, 0.66, 0.53, 0.50 and 0.33 respectively. As noted earlier, the hardening exponent (0.33) for 70.5° cases is closest to the room temperature hardening exponent values of steels. Thus we use two slip planes oriented ±70.5° to the crack plane in all the simulations reported here in this paper.

It should be noted that the plastic zone simulated here is generated from single sources emitting dislocations along each slip plane; where as the plastic zone in reality would be resulting from multiple sources and extended over many slip planes. However, this is a very good approximate model since as has been found in other simulations (Cleveringa et al. 2000; Noronha et al. 2000) even if randomly distributed active dislocation sources are allowed to operate in many slip planes, only few slip planes close to the crack-tip are shown to generate dislocations, or in other words, the plastic zone is found to be very narrow and coincident with the crack-tip. An added advantage or our method in comparison to (Cleveringa et al. 2000) is that the simulation in single slip plane allow us to "bundle dislocations" that are far away from the crack tip; there by enhancing the speed or our computation. Note in our method the applied load that could be reached in less than a week's computation is greater than 100 $\mathrm{MPam}^{1/2}$ where as the loads reported using the method in (Cleveringa et al. 2000) is less than 10 $\mathrm{MPam}^{1/2}$.

3.2 Calculation of microscopic fracture stresses (σ_F)

A through thickness crack of configuration shown on the right side of Fig. 1a is loaded monotonically in Mode-I, and dislocations are emitted along four symmetric slip planes oriented at $\alpha' = \pm 70.5°$ to the crack plane. Following an earlier study on the effect of source position (Roberts et al. 2002), we have chosen the source positions as $4b$, (b = 2.54 Å) along the slip planes. The stress fields of the emitted dislocations shield the crack-tip from the external load. Once moved to their equilibrium position, the amount of shielding from each dislocation is calculated using expressions from (Wang and Lee 1990), and the total shielding at each crack-tip is obtained by summation. The crack-tip stress intensity is calculated at each time step and when it reaches a critical value $k = K_{Ic}$ = 1.0 MPa$\sqrt{\text{m}}$ (value estimated for *Fe* with surface energy of 2 Jm^{-2}) (Price et al. 1964), the crack is assumed to propagate and the corresponding applied load is the microscopic fracture stress (σ_F).

The microscopic fracture stress (σ_F) is determined for a range of crack sizes from 0.1 to 5 μm. The fracture stresses (σ_F) determined for different temperatures for a given crack-length is shown in Fig. 4. It should be noted that the fracture stress (σ_F) of any given crack size vary only slightly with temperature, consistent with some experimental observations (e.g. Bowen et al. 1987). Note this slight increase in σ_F with temperature is in contrast to our earlier calculations (Roberts et al. 2002). The difference is in the slip plane angles chosen. In (Roberts et al. 2002) we considered dislocation emission along crystallographically plausible crack and slip planes, there by the number of dislocation emitted were less than that emitted for 70.5°. Considering only one of the most active slip planes obviously is an approximation and represents crack-tip plasticity confined to one single grain. However using 70.5° generates a plastic zone that is representative of plastic zone extended into several grains. Also, note the variation of σ_F we find is different from that assumed by Odette and He (Odette and He 2000) to explain the Master Curve. They used a constant σ_F at low temperature where the decrease in yield stress with temperature is rapid and an increasing σ_F at higher temperature where the yield stress variation with temperature is slow. Here, we find a montonic increase (though very marginal) in σ_F with temperature. The values of σ_F obtained and the corresponding mean friction stress is used to calculate the macroscopic fracture toughness (K_F).

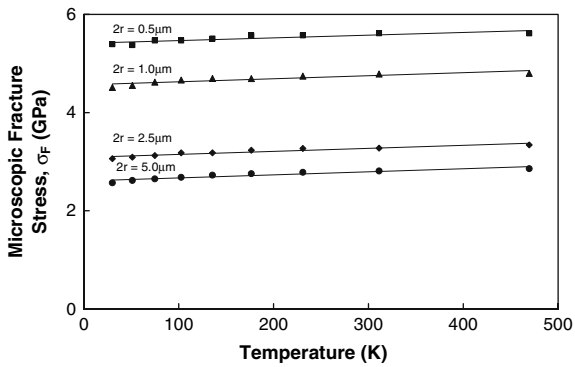

Fig. 4 The microscopic fracture stresses (σ_F) as a function of temperature for cases of four different microcrack sizes

3.3 Macrocrack simulation: calculation of fracture toughness (K_F)

Figure 5 shows typical behavior of the tensile stress (σ^p_{yy}) at the microcrack position X_P as a function of the applied load (K). The fracture criterion in the simulation is σ^p_{yy} reaching the critical value σ_F, (calculated in the previous stage) at X_P, the distance of the critical particle (microcrack) from the macrocrack tip. For the case shown here, the size of the

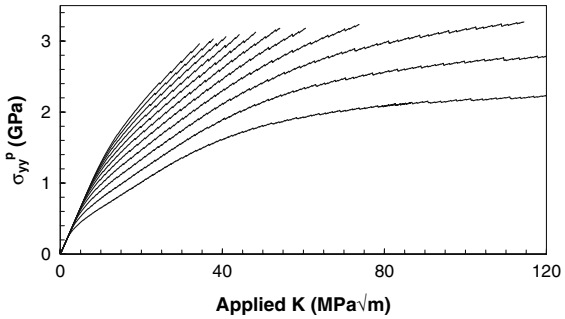

Fig. 5 The tensile stress at the microcrack (σ^p_{yy}) as a function of applied K for different temperatures. The temperature increases from left to right. The mean friction stress values corresponding to curves from left to right are 600–100 MPa at intervals of 50 MPa. (Note, the last two curves on the right may correspond to ductile regimes and only part of them are shown for clarity)

microcrack is 2.5 μm, the rate of loading, $dK/dt = 0.01$ MPa$\sqrt{\text{ms}^{-1}}$. As the temperature is increased the yield stress (or mean friction stress) is decreased, the applied stress intensity K required for the tensile stress at X_P to reach the critical value σ_F increases rapidly. Note the abscissa of the end point of each curve corresponds to the applied K at fracture (K_F); with increasing temperature, the K_F increase "exponentially". From left to right the curves correspond to decreasing yield stress or increasing temperatures. The two left most curves are displayed only partly for clarity; the last curve may correspond to limiting temperature at which cleavage fracture toughness can be estimated since the plastic zone size estimated for this case is larger than standard plane strain fracture test specimen sizes.

Thus, we can interpret the three major factors contributing to the sharp increase in fracture toughness with temperature as: (1) the decrease in tensile stress at the microcrack due to crack-tip blunting, (2) the increasing effects of a predominantly compressive stress field on the crack plane by emitted dislocations and (3) the increase in σ_F due to increase in microcrack tip plasticity with temperature. The effect of the first two factors can be seen in Figs. 6a–c, where the number of dislocations, the plastic zone size (d_F) and the radius of the blunted crack-tip (ρ_F) for each temperature measured at fracture, that is when K-applied = K_F is shown. The plastic zone size is the distance of the farthest dislocation from the crack-tip measured along the slip plane. The effect of increasing σ_F with temperature can be seen in Fig. 7a, which shows the macroscopic fracture toughness, K_F, as a function of temperature for cases with varying σ_F and for a constant σ_F. The squares represent fracture toughness estimated using σ_F calculated in the last section. For comparison K_F estimated using a constant $\sigma_F = 3$ GPa is also shown (marked diamond). The third curve shown is the K_F estimate with constant σ_F and without blunting of macrocrack tip. It should be noted that for the case without blunting, the fracture toughness (K_F) almost flattens at higher temperatures; similar to the predictions of (Ritchie et al. 1973). On the other hand, an increase in the fracture toughness is observed when blunting is accounted for in the simulation. The increase is even *sharper* when the slight variation found in σ_F estimates is also accounted. The finding emphasizes the significant effect of macrocrack tip

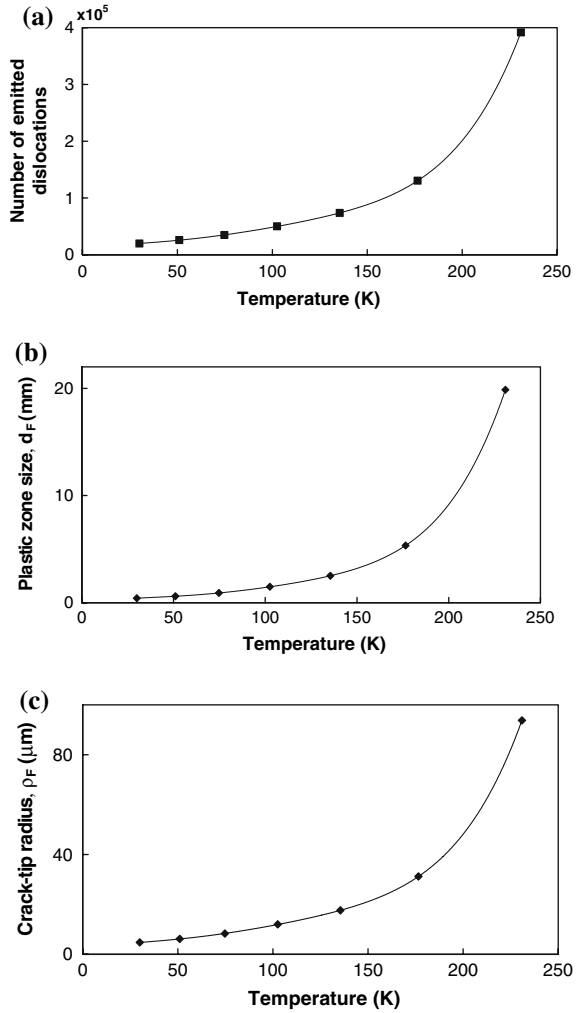

Fig. 6 (**a**) The number of dislocations emitted at fracture as a function of temperature (T). (**b**) The plastic zone size (d_F) calculated at K_F for each temperature is shown. (**c**) The crack-tip radius (ρ_F) and the plastic zone size (d_F) calculated at K_F for each temperature is shown

blunting in the increase of fracture toughness with temperature. Also the slight increase in σ_F further contributes to the rapid increase in fracture toughness with temperature. This sharp increase in the fracture toughness corresponds to the transition from brittle to ductile behavior. It should be noted that the estimated K_F shoots up beyond the data shown in Fig. 7a; however the corresponding d_F and ρ_F becomes too large to be accommodative in a fracture test specimen and may correspond to limiting temperatures where cleavage fracture toughness estimation is possible for the chosen conditions.

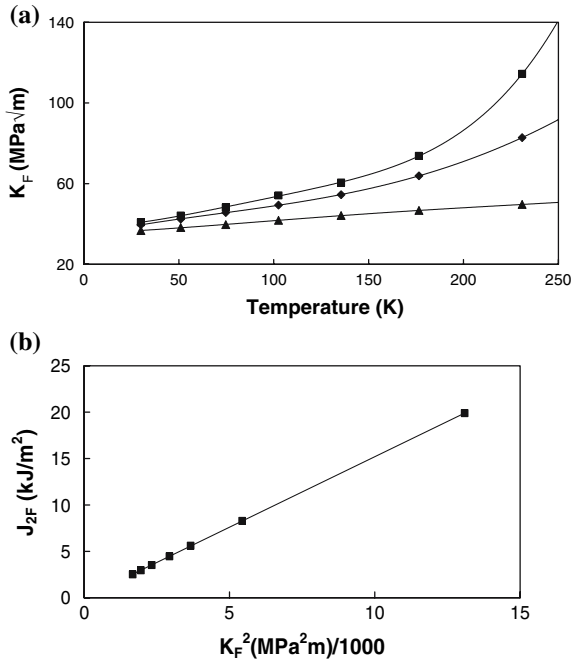

Fig. 7 (**a**) The fracture toughness (K_F) as a function of temperature for cases with and without blunting: microcrack size = 1 μm, X_p = 10 μm. (**b**) The J_{2F}—as a function of K_F^2 (estimated for different temperatures) is shown

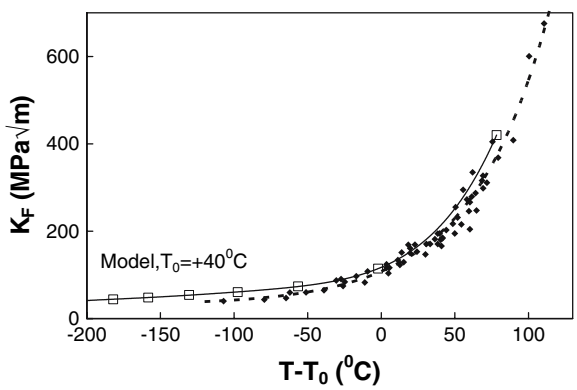

Fig. 8 The estimated fracture toughness (K_F) values are plotted along with experimental data and Master curve reported in (Wallin 1993)

In Fig. 7b the J_{2F}, the J_2—integral value at fracture, calculated from the number of dislocations emitted at the corresponding load K_F is shown. J_2 is defined as the sum of the glide forces on all dislocations around the crack-tip (Shi et al. 2004). In this case, the dislocations are in equilibrium against the friction stress (τ_y) and we can compute J_{2F} as the product of the total number of dislocations (N) and the friction stress (τ_y). Considering the fact that J_{2F} is calculated from the number of dislocations emitted at applied stress intensity, K_F, it is striking to note that the linear relation between J_{2F} and K_F^2 is perfectly obeyed.

3.4 Comparison with experiments (Master Curve Data)

To compare our model with existing experimental data, we plot the data set used to construct the Master Curve (MC) originally (Wallin 1993). According to the MC hypothesis, the shape of the brittle–ductile transition curve is universal for all steels and can be expressed by a single expression of the form $K(T_0) = 31\text{MPa}\sqrt{m} + 70\text{MPa}\sqrt{m}.\exp\{0.019/^\circ C\ (T - T_0)\}$ where T_0 is the reference temperature specific to a material and T is the temperature in °C. Thus all fracture toughness data of ferritic steels can be collapsed to this curve using an appropriate T_0 specific to the material. In Fig. 8, the fracture toughness data compiled and reported by Wallin in (Wallin 1993), is shown along with fracture toughness values calculated using our model. The diamond symbols correspond to experimental data points, and the broken line shown is the Master Curve. The toughness values calculated using our model (the open squares connected by solid line) is plotted along side using a reference temperature, T_0 = + 40°C. The T_0 value is chosen arbitrarily to move the model curve to the MC; however it should be noted that the shape of the transition curve is not affected by T_0. It is remarkable to note that the shape of the model curve is very similar to the Master Curve, thus infact the model proposes a physical basis to this empirical relation.

4 Summary and conclusions

The fracture of ferritic steels involves a macrocrack with microcracks ahead of it in its crack plane; we performed a two dimensional dislocation simulation of this system. The stress field along the crack plane (y = 0) obtained by our simulations for a plain strain semi-infinite blunted crack is comparable to the HRR field along the crack plane. We calculated the fracture

toughness at different temperatures by inputting the corresponding yield stress which in turn determines the friction stress for dislocation motion. The sharp increase in fracture toughness around the brittle–ductile transition temperature is found to be a combined effect of the following factors: (a) the increase in mobility of emitted dislocations with temperature, (b) the decrease in tensile stress along the crack plane due to crack-tip blunting and the compressive stresses on the crack-plane due to the emitted dislocations from the marcocrack, and (c) the increase in microcrack-tip plasticity and the consequent increase in σ_F with temperature. The mobility of emitted dislocations determines the equilibrium position of dislocations and thus determines the tensile stress at the microcrack. Also the mobility of dislocations around the microcrack determines the crack-tip stress intensity at the microcrack, and thus the microscopic fracture toughness (σ_F), which ultimately determines the fracture toughness of the material (K_F). As can be seen in Fig. 7a, even though the blunting alone loads to an upturn of the transition curve that is not sufficient to produce a sharp increase in fracture toughness as observed in experiments. The increasing σ_F with temperature contributes to even sharper upturn at the transition. The model compares well with the Master Curve data; using a reference temperature the model is compared with the Master Curve, thus proposing a physical basis for the Master Curve.

Acknowledgements This work is supported by the US Department of Energy, Office of Fusion Energy, through Grant DE-FG02-03ER54708 with UCLA.

References

ASTM Standard Test Method E 1921-02: Standard Test Method for Determination of Reference Temperature, T_0, for Ferritic Steels in the Transiton Range. Annual Book of ASTM Standards, vol. 03.01, p 1139–1163

Beremin, F.M.: Local criterion for cleavage fracture of a nuclear pressure vessel steel. Metall. Trans. A **14**, 2277–2287 (1983)

Bowen, P., Druce, S.G., Knott, J.F.: Effects of microstructure on cleavage fracture in pressure vessel steel. Acta Metall. **34**, 1121 (1986)

Bowen, P., Druce, S.G., Knott, J.F.: Micromechanical modelling of fracture toughness. Acta Metall. **35**, 1735–1746 (1987)

Bowen, P., Knott, J.F.: Size effects on the microscopic cleavage fracture stress, σ^*, in martensitic microstructures. Metall. Trans. A **17**, 231–241 (1986)

Cleveringa, H.H.M., Van der Giessen, E., Needleman, A.: Discrete dislocation analysis of mode I crack growth. J. Mech. Phys. Solids **48**, 1133–1157 (2000)

Creager, M., Paris, P.C.: Elastic field equations for blunt cracks with reference to stress corrosion cracking. Int. J. Frac. Mech. **3**, 247–252 (1967)

Curry, D.A., Knott, J.F.: Effect of microstructure on cleavage fracture toughness of quenched and tempered steels. Met. Sci. **13**, 341–345 (1979)

Hirsch, P.B., Roberts, S.G.: Brittle-ductile transition in silicon. Phil. Mag. A **64**, 55–80 (1991)

Hirsch, P.B., Roberts, S.G.: Modelling crack tip plastic zones and the brittle-ductile transition. Phil. Trans. R. Soc. Lond. A **355**, 1991–2001 (1997)

Hirsch, P.B., Roberts, S.G., Samuels, J.: The brittle-ductile transition in silicon-II. Interpretation. Proc. R. Soc. Lond. A **421**, 25–53 (1989)

Hutchinson, J.W.: Singular behaviour at the end of a tensile crack in a hardening material. J. Mech. Phys. Solids **16**, 13–31 (1968)

Lakshmanan, V., Li, J.C.M.: Edge dislocations emitted along inclined planes from a mode I crack. Mater. Sci. Eng. A **104**, 95–104 (1988)

McMahon, C.J. Jr, Cohen, M.: Initiation of cleavage in polycrystalline Iron. Acta Metall. **13**, 591–604 (1965)

McMeeking, R.M.: Finite deformation analysis of crack-tip opening in elastic-plastic materials and implications for fracture. J. Mech. Phys. Solids **25**, 357–381 (1977)

Natishan M.E., Kirk M.T.: Micromechanical evaluation of the Master Curve. In: Paris, P.C., Jerina, K.L. (eds.) Fatigue and Fracture Mechanics, vol. 30, p. 51–60. ASTM STP 1360, ASTM, West Conshohocken, PA (2000)

Noronha, S.J., Ghoniem, N.M.: Dislocation simulation of brittle-ductile transition in ferritic steels. Metall. Mater. Trans. A **37**, 539–544 (2006)

Noronha, S.J., Roberts, S.G., Wilkinson, A.J.: Multiple slip plane model for crack-tip plasticity. In: Robertson, I.M. et al. (eds.) MRS Proceedings 578, Multiscale Phenomena in Materials—Experiments & Modeling, pp. 309–314. MRS, Warrendale, PA (2000)

Odette, G.R., He, M.Y.: A cleavage toughness Master Curve model. J. Nucl. Mater. **283–287**, 120–127 (2000)

Orowan, E.: Physics of fracture. Trans. Inst. Engrs. Shipbuilders in Scotland **89**, 165–215 (1945)

Ortner, S.R., Hippsley, C.A.: Two component description of ductile to brittle transition in ferritic steel. Mater. Sci. Tech. **12**, 1035–1042 (1996)

Price, A.T., Hall, H.A., Greenough, A.P.: The surface energy and self diffusion coefficient of solid iron above 1350°C. Acta Metall. **12**, 49–58 (1964)

Rice, J.R.: Dislocation nucleation from a crack tip: an analysis based on the Peierls concept. J. Mech. Phys. Solids **40**, 239–271 (1992)

Rice, J.R., Rosengren, G.: Plain strain deformation near a cack tip in a power-law hardening material. J. Mech. Phys. Solids **16**, 1–12 (1968)

Rice, J.R., Thomson, R.M.: Ductile versus brittle behaviour of crystals. Phil. Mag. **29**, 73–97 (1974)

Ritchie, R.O., Knott, J.F., Rice, J.R.: On the critical relationship between critical tensile stress and fracture toughness in mild steel. J. Mech. Phys. Solids **21**, 395–410 (1973)

Roberts S.G.: Modelling the brittle to ductile transition in single crystals. In: Kirchner, H.O., Kubin, L.P., Pontikis, V. (eds.) Computer Simulation in Materials Science-nano/meso/macroscopic Space and Time Scales, NATO ASI Series 308, pp. 409–434 (1996)

Roberts, S.G., Noronha, S.J., Wilkinson, A.J., Hirsch, P.B.: Modelling the initiation of cleavage fracture of ferritic steels. Acta Mater. **50**, 1229–1244 (2002)

Saka, H., Nada, K., Imura, T.: Tensile test of foil specimens of iron single crystals at room and low temperatures under observation in high voltage electron microscope. Cryst. Latt. Def. **4**, 45–56 (1973)

Shi, M.X., Huang, Y., Gao, H.: The J-integral and geometrically necessary dislocations in nonuniform plastic deformation. Int. J. Plasticity **20**, 1739–1762 (2004)

Stoller, R.E., Zinkle, S.J.: On the relationship between uniaxial yield strength and resolved shear stress in polycrystalline materials. J. Nucl. Mater. **283–287**, 349–352 (2000)

Veistinen, M.K., Lindroos, V.K.: Evaluation of the effective surface energy of ferrite in a 26 Cr-1 Mo ferritic stainless steel. Scripta Metall. **18**, 185–188 (1984)

Wallin, K.: Irradiation damage effects on the fracture toughness transition curve shape for reactor pressure vessel steels. Int. J. Pres. Ves. & Piping **55**, 61–79 (1993)

Wallin, K., Saario, T., Törrönen, K.: Statistical model for carbide induced brittle fracture in steel. Metal. Sci. **18**, 13–16 (1984)

Wang, S., Lee, S.: Analysis of the elastic interaction between an edge dislocation and an internal crack. Mater. Sci. Eng. A **130**, 1–10 (1990)

Zerilli, F.J., Armstrong, R.W.: Dislocation-mechanics-based constitutive relations for material dynamics calculations. J. Appl. Phys. **61**, 1816–1825 (1986)